

# Nanoscale-Resolved Spatial Mapping of Tip-Mediated Terahertz Emission from Semiconductors

Angela Pizzuto<sup>1</sup> · Enrique Castro-Camus<sup>2</sup> · Daniel M. Mittleman<sup>3</sup>

Received: 30 November 2022 / Accepted: 27 January 2023 © The Author(s), under exclusive licence to Springer Science+Business Media, LLC, part of Springer Nature 2023

#### **Abstract**

Scattering-type scanning near-field optical microscopy (s-SNOM) has become a powerful tool for subwavelength-resolved imaging and optical spectroscopy. The technique is particularly useful in the terahertz or other long-wavelength regimes, where the diffraction limit prohibits resolving even micron-sized objects. This approach can also drastically improve the spatial resolution of nonlinear measurements such as laser terahertz emission microscopy (LTEM), in which a broadband THz pulse is generated after photoexcitation by a near-infrared (NIR) pulse. However, in all prior near-field LTEM experiments, the pump spot has been localized to the scattering probe, to couple to the generated THz radiation at the center of the illuminated region. Here, we demonstrate the first nonlocal near-field LTEM experiments, in which an ultrafast NIR pulse photoexcites a sample at a location that is laterally shifted from the location of the near-field probe which couples the THz signal to the far field. Increasing lateral shifts of the pump spot produce larger time delays in the arrival of the emitted broadband THz pulse, consistent with drift of the subsurface dipole between the pump location and probe tip. Monte Carlo simulations corroborate the time shift for the dipole formation, which in turn produces the THz emission with a relative delay. The simulation results show excellent agreement with experiments. This nonlocal s-SNOM approach to LTEM offers a new opportunity for studying lateral transport on the nanoscale and may be particularly useful in anisotropic materials.

**Keywords** Terahertz · Ultrafast optics · s-SNOM · Near-field microscopy

Published online: 07 February 2023



Department of Physics, Brown University, Providence, RI 02912, USA

Department of Physics, University of Marburg, 35037 Marburg, Germany

School of Engineering, Brown University, Providence, RI 02912, USA

#### 1 Introduction

For decades, terahertz time-domain spectroscopy (THz-TDS) and imaging have been widely used for characterizing charge carrier behavior in a variety of materials relevant to the fields of biology [1–3], materials physics [4, 5], and chemistry [6, 7]. Unlike pulse characterization methods in other wavelength regimes, the electric field of the THz pulses is detected in the time domain, so all spectral information can be retrieved via Fourier transform [8, 9]. THz-TDS is especially useful for characterizing the optoelectronic properties of semiconductors; their plasma frequencies often occur in the terahertz regime, providing distinct spectral signatures in devices which are important in modern electronics [10]. Moreover, with a photon energy far below the band gap of conventional semiconductors, THz radiation allows for a noninvasive measurement of only the carriers which already contribute to conductivity. However, the spatial resolution of conventional THz-TDS is low; because of the diffraction-limit, THz images cannot resolve objects with dimensions smaller than hundreds of micrometers. Scattering-type scanning near-field optical microscopy (s-SNOM) is capable of bypassing this limit [11, 12]. A sharp, metallic probe tip sits nanometers above the surface of the sample, spatially confining incident light near its apex to a spot whose size is on the order of the tip radius. This can be tens of nanometers wide, orders of magnitude smaller than the incident wavelength. This idea has been groundbreaking for nanoscale characterization of bulk semiconductors [13, 14], nanostructures [13, 15–19], topological insulators [20, 21], and 2D materials [4, 5, 22, 23] using THz radiation. Furthermore, in addition to linear optical measurements, a s-SNOM approach can also greatly improve the spatial resolution of nonlinear optical imaging techniques such as laser terahertz emission microscopy (LTEM) [24-26]. LTEM is well known to be a powerful tool for examining photo-induced charge carrier dynamics in solids, with applications in the evaluation of integrated circuits and solar cells, but it has only recently been adapted to the s-SNOM technique [27–29] to enable nanoscale spatial resolution. Moreover, while prior studies of near-field LTEM have successfully extracted local properties of the material directly underneath the metal tip, there is significant and so far unexplored value in measuring *nonlocal* phenomena in the near field [30, 31].

In this paper, we demonstrate the first nonlocal near-field LTEM experiment. In our measurements, an ultrafast near-infrared (NIR) pulse photoexcites a semiconductor at a location that is laterally shifted from the metallic tip, creating a subsurface dipole that evolves after the arrival of the optical pulse. This optically induced dipole generates broadband terahertz emission, which is outcoupled from the surface at the location of the near-field probe. We observe that increasing the lateral distance between the tip and the pump spot leads to increasing delays in the arrival time of the THz pulse at the detector. This delay is consistent with vertical and lateral diffusion of the NIR-induced subsurface dipole from the pump spot to the location of the tip. These results, which require a near-field approach (as micron-sized diffusion lengths would be impossible to resolve in the far field using THz radiation), suggest many new opportunities for studying electronic and structural anisotropy on the nanoscale.



#### 2 Results and Discussion

Our s-SNOM measurements use an atomic force microscope (AFM) and PtIr-coated probe tips with ~40 nm tip radius and 80 µm shank length to measure THz emission from the sample substrate via near-field THz time-domain spectroscopy (THz-TDS) [9, 32, 33]. Near-infrared (NIR) pulses (~100 fs) with 820 nm center wavelength are generated by a Ti:sapphire oscillator, with 80 MHz repetition rate. The laser beam is focused to a diffraction-limited spot on the tip-sample area with an off-axis parabolic mirror inside the AFM. THz radiation emitted from the sample is detected coherently outside of the AFM using free-space electro-optic (EO) sampling with a lock-in amplifier referenced to a harmonic of the tip-tapping frequency (~23 kHz). Any excess NIR radiation scattered forward from the sample is blocked from the detection crystal (2 mm thick ZnTe) with a thin layer of Teflon to ensure proper THz pulse detection. For this experiment, we measure full THz time-domain waveforms at incremental lateral shifts of the pump spot to map the changing THz emission strength of the sample directly at the AFM probe tip location [34]. We measure waveforms demodulated at the 2<sup>nd</sup> harmonic of the tip tapping frequency for an adequate signal-to-noise ratio and appropriate suppression of the far-field background radiation [35–37].

The lateral position of the pump spot is controlled independently of the tip and sample positions; immediately before entering the AFM, the NIR pump is reflected off an external motorized mirror (shown in Fig. 1a), whose pitch can be repositioned with 1.1 arcsecond angular resolution. We estimate, from a ray matrix analysis of the AFM internal optics, that this corresponds to a minimum lateral shift for the pump spot on the sample surface of approximately 55 nm; this is about the same as the size of the AFM tip and is small compared to the ~1.3  $\mu$ m diameter of the pump beam spot at the sample surface. When the NIR beam spot is spatially coincident

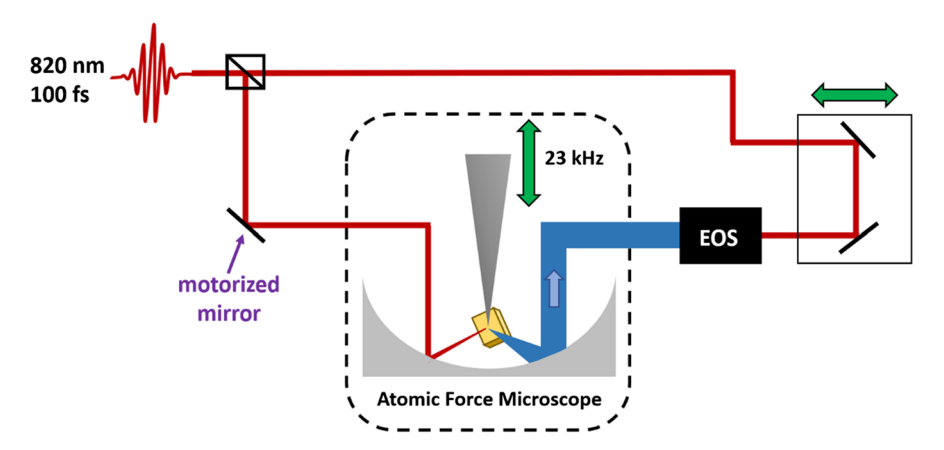


Fig. 1 Schematic of NIR path and near-field LTEM experiment. A Ti:sapphire laser generates ultrafast near-infrared pulses which generate THz emission from a semiconductor sample inside an atomic force microscope. Emitted single-cycle terahertz pulses are detected in the time domain via electro-optic sampling



with the AFM tip, we refer to this as a "local" positioning (Fig. 2a, left). A "nonlocal" positioning is one in which the pump has been laterally offset, such that carriers are required to travel between the pump and probe tip location to reach the probed volume (as shown on the right side of Fig. 2a, b).

We compare our local and nonlocal LTEM experiments on two featureless InAs wafers, which have specified p-doping levels of approximately  $10^{16}\ cm^{-3}$  and  $10^{18}\ cm^{-3}$ . Using the external positioning mirror, we first position the pump directly under the tip and measure the near-field THz emission, as in all previous near-field LTEM measurements. We then laterally displace the pump spot away from this "local" positioning, in increments of 200–250 nm, up to a maximum displacement of approximately  $2\ \mu m$ .

For both the lightly doped (Fig. 3a) and more heavily doped (Fig. 3b) InAs wafers, we observe a clear delay in the arrival time of the emission pulses, correlating monotonically with increasing lateral offsets of the NIR spot. In both samples, a 2  $\mu$ m pump spot shift creates an approximately 500 fs delay in the arrival of the LTEM pulse. This corresponds to an average lateral dipole diffusion speed of  $4 \times 10^6$  m/s. If we assume all excess pump energy—above the InAs bandgap—is transferred into kinetic energy, a simple velocity calculation using the effective mass of electrons in InAs  $(0.023m_0)$  yields an approximate carrier velocity of  $4.2 \times 10^6$  m/s. While approximate, this calculation strongly suggests that we are

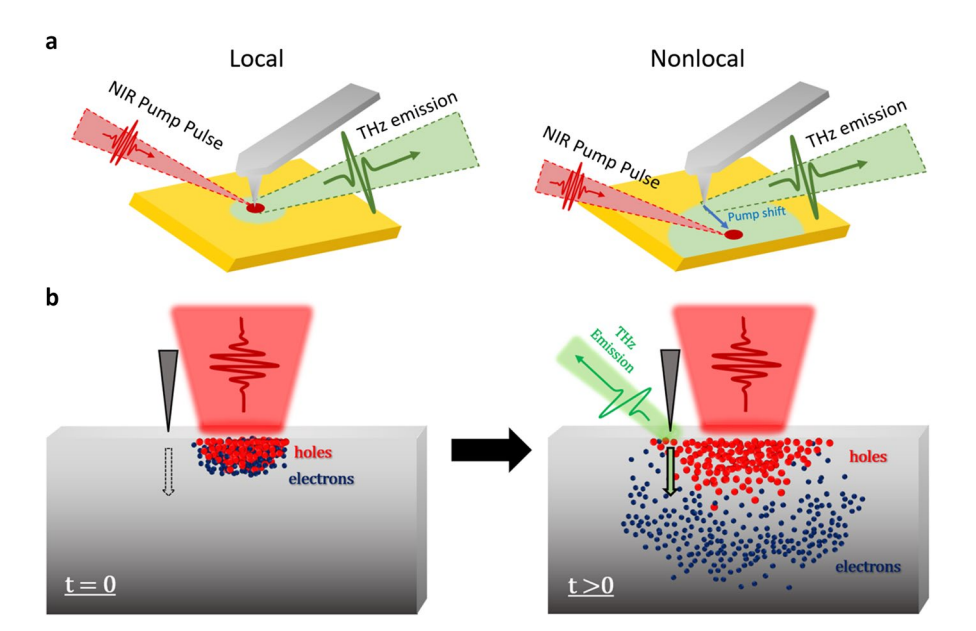


**Fig. 2** a Left: schematic of standard LTEM experiment, where the pump is focused directly underneath the AFM probe tip. Right: schematic of "nonlocal" near-field LTEM experiment, where the pump spot on the sample is laterally shifted relative to the AFM tip, to capture carrier transport effects. **b** Schematic of the AFM tip in a "nonlocal" position at t = 0 (the instant of NIR pulse arrival) and t >> 0—when the photo-Dember dipole has diffused so there is a vertical component of the dipole directly underneath the tip. At this point, at some t >> 0, we measure a nonlocal LTEM signal with an arrival time which is delayed relative to a "local" tip positioning



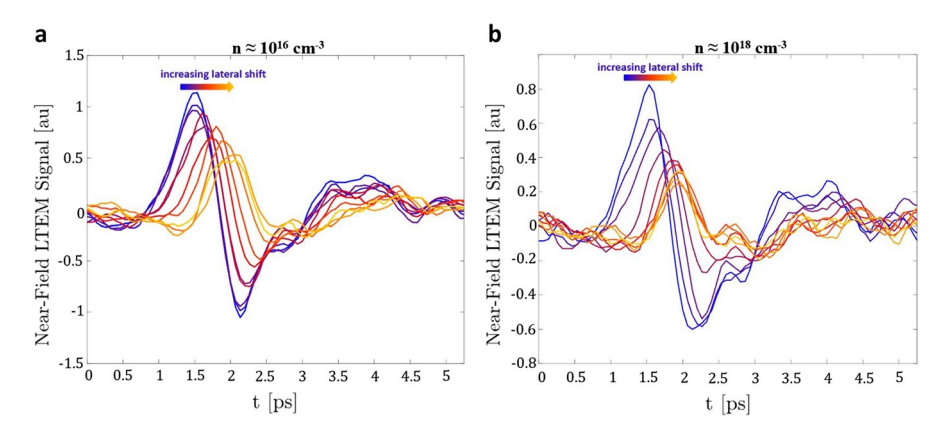


Fig. 3 Local and increasingly nonlocal near-field LTEM measurements. a On lightly p-doped InAs,  $n \approx 10^{16}~\text{cm}^{-3}$ . b On more heavily doped p-InAs,  $n \approx 10^{18}~\text{cm}^{-3}$ . Increasingly warmer colors correspond to larger lateral pump offsets, up to a maximum displacement of approximately 2  $\mu$ m

directly measuring carrier drift and diffusion using this nonlocal LTEM technique. We also observe weaker emission as the pump offset increases, consistent with our expectation that a smaller portion of the photo-Dember dipole is outcoupled by the tip as the offset increases. We note that the overall emission is weaker in the more highly doped InAs; this is to be expected, as the higher concentration of carriers lowers the absorption of the pump beam while also inhibiting the outcoupling of the THz pulse from below the sample surface into the air.

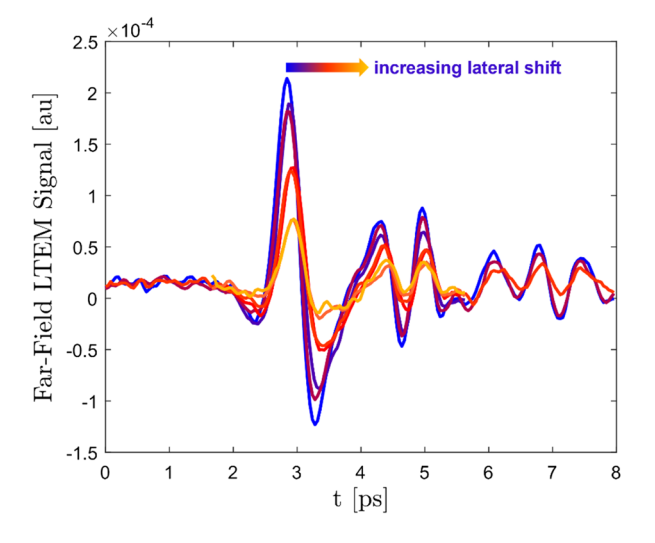
Because carrier mobility is generally inversely related with concentration, we might expect naively that the same lateral pump shifts would cause much larger delays in the arrival time for the highly doped sample relative to the lightly doped sample; that is, the photo-Dember dipole would diffuse much more slowly in the highly doped sample, causing much later THz emission in the near field. However, we observe that this is not the case; the relationship between arrival times and lateral pump offsets is nearly the same between highly and lightly doped samples, suggesting that this simple explanation is insufficient. In fact, we are exciting photocarriers very high above the 0.35 eV band gap of InAs; it is these hot carriers that are responsible for the emission of THz radiation. Their initial kinetic energy, and therefore their velocity during the current transient, depends on their location high above the bottom of the conduction band and is not so sensitive to the population of background cold carriers. It is therefore not surprising that the times associated to the transport of these hot carriers are comparable, regardless of the intrinsic carrier concentration, as reflected by the comparable time delays observed in Fig. 3. The most obvious difference between Fig. 3a and 3b is in the amplitudes of the emitted THz pulses; in the highly doped sample, the emitted THz pulses weaken much more rapidly with increasing pump shift. This is where the higher doping concentration has its clearest effect. Cold carriers may screen local fields and reduce the strength of the photo-induced dipole. Moreover, hot photocarriers are much more likely to collide with cold carriers when the doping is higher, causing a "decoherence" in



the current; these collisions increase the likelihood that photoexcited carriers change their direction of motion, making them less likely to arrive at the tip within a given timeframe and causing a weakening of the near-field THz emission. These effects are unrelated to the relationship between background carrier concentration and excitation density [38], which we estimate to be approximately  $2 \times 10^{19}$  cm<sup>-3</sup> in our experiment. Indeed, the nonlocal LTEM technique described here provides a unique window on these complex carrier dynamics.

Before attempting to extract more rigorous quantitative results, we first consider the possibility that, by tilting our motorized mirror, we are gradually increasing the optical path length that the NIR pump pulse must travel before it arrives at the sample surface; this would induce a similar shift in arrival time which would be unrelated to carrier motion and may confound our measurements. To ensure that this is not the case, we perform identical measurements in the far field. We retract the tip from the sample—far enough so that there is no near-field interaction—and measure the arrival time of the emitted THz pulses by referencing our lock-in to an optical chopper which modulates the incoming pump beam at 3.17 kHz. This measurement would reveal only the time delay resulting from such trivial optical path length changes, if one were present. As shown in Fig. 4, we observe that, for the identical set of lateral pump shifts in Fig. 3, the far-field LTEM pulses all arrive at nearly the same time. This demonstrates that varying the mirror tilt induces no significant change in path length, and the delay we observe in the near field is truly due to carrier dynamics after photoexcitation. Additionally, in the case of a path length increase, we would not expect the near-field peak-to-peak amplitudes to decrease as significantly as they do in our data. The decrease in THz field strength with increasing pump shift shown in Fig. 4 is certainly a result of changing alignment; when the pump spot is shifted and therefore not focused directly underneath the tip apex, portions of the NIR beam or the outgoing THz beam may be blocked by the tip and cantilever. In both cases, this would cause a reduced THz amplitude. Conversely,

Fig. 4 Optically chopped p-InAs LTEM signal, showing no optical path length changes associated with lateral shifts in the pump spot





because of the antenna properties of the tip, this type of alignment issue is not present in the near field, because the measured signal always originates from the same location (the tip), and background radiation is filtered by higher-harmonic demodulation. We also note that, in the prior works studying near-field LTEM, it has been suggested that the tip acts as a nanoprobe, outcoupling THz radiation from a small region, rather than as a nanopump, inducing a subsurface dipole on the nanoscale. The results shown here confirm this earlier conclusion that the tip's primary role *must* be that of a nanoprobe; to observe the shifts in arrival time shown in Fig. 3, it is required that the tip outcouples only the edges of an extended subsurface carrier distribution. If instead its role was as a nanopump, the emission would always be centered at the probe tip, and we would observe no time delay with increasing lateral pump shift. So, in addition to providing an enhanced picture of carrier properties in the InAs, this nonlocal LTEM experiment has provided added clarification for the near-field LTEM mechanism.

In order to quantitatively corroborate the experimental results shown in Fig. 3, we perform a semiclassical Monte Carlo simulation [38] of the diffusing subsurface dipole in lightly doped InAs after the carriers have been photoexcited by an ultrafast NIR pulse. We simulate the motion of five million quasiparticles representing electrons and holes. Each particle is advanced classically in one femtosecond timestep, at each step scattering probabilities are calculated for a variety of mechanisms and a quasirandom number determines its scattering probability, its scattering angle, energy gain/loss, and if it recombines or becomes trapped. The particle density is calculated and used to solve the Poisson equation at each step; this determines the local electric field which influences particle motion for the subsequent timestep. The InAs is assumed to be at room temperature (300 K) and to have a very low intrinsic carrier concentration (10<sup>14</sup> cm<sup>-3</sup>). Although this is not equal to the carrier concentration of our real samples ( $10^{16}$  cm<sup>-3</sup>,  $10^{18}$  cm<sup>-3</sup>), we note that adding more carriers is computationally very expensive. Moreover, InAs wafers with low concentrations of  $10^{14}$  cm<sup>-3</sup> and  $10^{16}$  cm<sup>-3</sup> can be expected to exhibit very similar behavior. In order to simulate the arrival of the NIR pulse, photocarriers are injected using quasirandom numbers following a temporal and spatial Gaussian distribution (FWHM 100 fs and 1 µm) and an exponential distribution in the direction normal to the surface ( $a = 1.2 \mu m$ ). Further details about the simulation can be found in prior works [38, 39].

The strength of the emitted THz field is proportional to the gradient of the vertical photocurrent generated by the NIR pump [40]; we track this quantity as a function of distance from the pump spot and recreate the expected arrival times and peak-to-peak amplitudes of the LTEM signal. To illustrate this, we plot the vertical photocurrent ( $J_z$ ) and subsequent THz emission pulse as a function of time for some selected pump offsets in Fig. 5. Figure 5b shows the predicted THz emission field, calculated from the gradient of the data in Fig. 5a. The dotted lines are values extracted directly from the simulation, and solid lines are error function fits to smooth the unphysical numerical noise of the simulation. We observe that the simulation shows the same qualitative trends as our experimental data; as the pump shift increases, the strength of the vertical photocurrent and subsequent THz emission decreases, and the arrival time delay increases. However, we note that the simulation



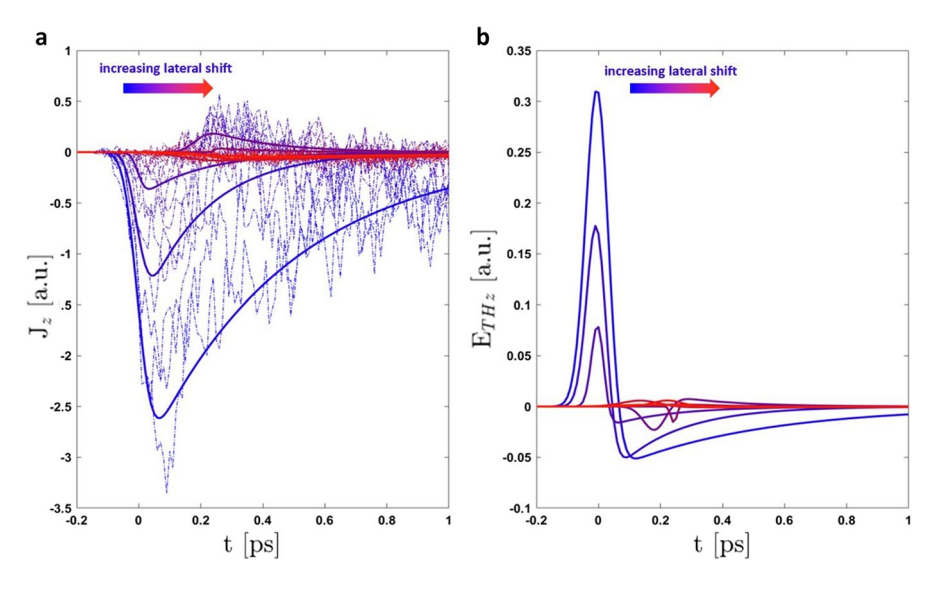
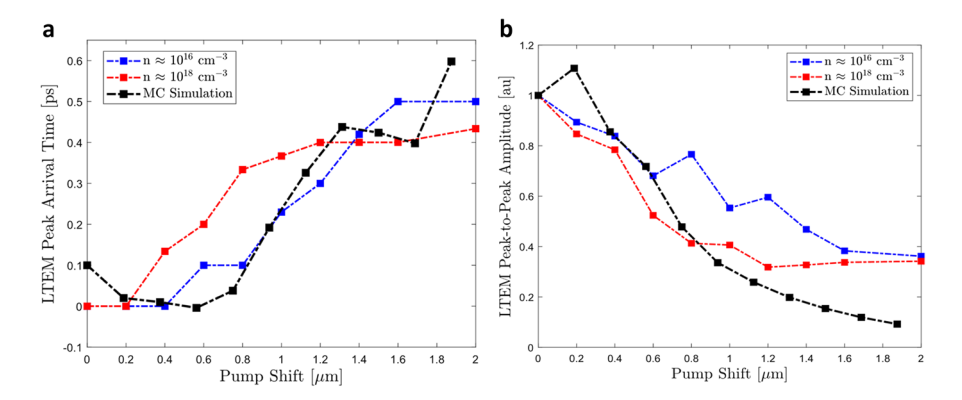


Fig. 5 a Monte Carlo simulation of vertical subsurface current  $J_z$  induced by photoexcitation by an ultrafast NIR pulse and the photo-Dember effect in InAs. Different curves correspond to different lateral pump shifts away from the nanotip in increments of approximately 70 nm. Dotted curves show raw simulation results, while Gaussian fits for clarity are shown as the solid lines. **b** Simulated THz emission pulse, obtained by taking the negative gradient of (a)

predicts a more rapid decay than observed in either InAs wafers; this causes the photocurrent and subsequent emission pulses to become too small to visualize in Fig. 5, once the pump offset exceeds approximately 1 µm. This discrepancy is likely a result of the conditions and interpretation of the simulation; it is important to note that our simulation represents the photoexcitation characteristics of lightly doped InAs in the far field; the tip's effect on the outcoupled signal, as well as its direct modulation of the local dielectric function of the sample, is not accounted for. In Fig. 6, we extract the arrival time delay and peak-to-peak THz amplitudes from the full simulation and directly compare them to our data. We find excellent agreement between our experimental arrival time shifts for 10<sup>16</sup> cm<sup>-3</sup> InAs (Fig. 6a, blue line) and our Monte Carlo simulation (Fig. 6a, black line), suggesting that the nonlocal LTEM technique is effective in measuring charge carrier transport properties which are not observable with traditional "local" near-field techniques. Additionally, our simulation does not account for the finite detection bandwidth of the ZnTe crystal which suppresses frequencies above 2.2 THz; our amplitude prediction incorporates these higher frequencies—which decay very rapidly with pump offset—while our experiment does not. Indeed, we observe that our simulated THz pulses change shape appreciably as the pump offset increases. For this reason, we choose to measure the arrival times of our simulated pulses by the time at which the vertical photocurrent is maximized, i.e., the zero-crossing point of the emission pulses between their positive and negative peaks. This allows us to reliably track changes in the pulse timing without requiring a consistent pulse shape. Moreover, the qualitative behavior of the peak-to-peak amplitudes of the signals from the lightly doped InAs (Fig. 3b,





**Fig. 6** a Lateral pump shift vs. LTEM pulse peak arrival time in lightly doped InAs (blue), more heavily doped InAs (red), and in simulation (black). **b** Lateral pump shift vs. emitted THz pulse peak-to-peak E field strength for lightly doped InAs (blue), heavily doped InAs (red), and in simulation (black)

blue), heavily doped InAs (Fig. 6b, red), and simulation (Fig. 6b, black) agrees well. Although not perfect, the good agreement in Fig. 6 indicates that the tip does not strongly perturb the observed dynamics.

## 3 Conclusion

In summary, we present the first nonlocal near-field laser terahertz emission microscopy measurements on lightly and heavily doped bulk InAs wafers. We find that a lateral shift in the pump spot relative to the nanotip yields a time-shifted emission response consistent with hot carrier ballistic transport after photoexcitation, as well as surface field-induced drift. Numerical Monte Carlo simulations of photoexcited carriers in lightly doped InAs confirm the relation between pump shift and LTEM pulse arrival time delay and peak amplitude. This technique is a valuable addition to the range of near-field THz spectroscopy and imaging techniques and may be of particular interest for measuring carrier dynamics in materials with anisotropic transport properties.

**Author Contribution** A. Pizzuto performed all experiments and data analysis, wrote the main manuscript text, and prepared all figures. E. Castro-Camus performed associated computational simulations. D. Mittleman was responsible for significant intellectual contributions, securing funding, and providing resources for the experimental procedures. All authors reviewed and edited the manuscript fully, and all authors have approved the final submission.

**Funding** This work has been supported by grants from the US National Science Foundation Division of Electrical Communications and Cyber Systems. ECC would like to thank the support from the Alexander von Humboldt Foundation through an Experienced Research Fellowship.

Data Availability All data presented in this study is available from the corresponding author upon request.



### Declarations

**Ethics Approval** This research did not include studies involving human or animal subjects. No specific permissions or approvals were required.

**Competing Interests** The authors declare no competing interests.

#### References

- Novelli, F. et al. Time-Domain THz Spectroscopy Reveals Coupled Protein-Hydration Dielectric Response in Solutions of Native and Fibrils of Human Lysozyme. The Journal of Physical Chemistry B 121, 4810-4816, https://doi.org/10.1021/acs.jpcb.7b02724 (2017).
- Solemanifar, A. et al. Probing peptide nanowire conductivity by THz nanoscopy. Nanotechnology 33, 065503, https://doi.org/10.1088/1361-6528/ac34a6 (2021).
- Niessen, K. A. et al. Protein and RNA dynamical fingerprinting. Nature Communications 10, 1026, https://doi.org/10.1038/s41467-019-08926-3 (2019).
- 4. Stinson, H. T. *et al.* Imaging the nanoscale phase separation in vanadium dioxide thin films at terahertz frequencies. *Nature Communications* **9**, 3604, https://doi.org/10.1038/s41467-018-05998-5 (2018).
- Zhang, J. et al. Terahertz Nanoimaging of Graphene. ACS Photonics 5, 2645-2651, https://doi. org/10.1021/acsphotonics.8b00190 (2018).
- 6. Neu, J. et al. Terahertz Spectroscopy of Tetrameric Peptides. *The Journal of Physical Chemistry Letters* **10**, 2624-2628, https://doi.org/10.1021/acs.jpclett.9b01091 (2019).
- Neu, J., Nikonow, H. & Schmuttenmaer, C. A. Terahertz Spectroscopy and Density Functional Theory Calculations of dl-Norleucine and dl-Methionine. *The Journal of Physical Chemistry A* 122, 5978-5982, https://doi.org/10.1021/acs.jpca.8b04978 (2018).
- 8. van Exter, M., Fattinger, C. & Grischkowsky, D. Terahertz time-domain spectroscopy of water vapor. *Opt. Lett.* **14**, 1128-1130, https://doi.org/10.1364/OL.14.001128 (1989).
- 9. Aghamiri, N. A. et al. Hyperspectral time-domain terahertz nano-imaging. Opt. Express 27, 24231-24242, https://doi.org/10.1364/OE.27.024231 (2019).
- Huber, A. J., Keilmann, F., Wittborn, J., Aizpurua, J. & Hillenbrand, R. Terahertz Near-Field Nanoscopy of Mobile Carriers in Single Semiconductor Nanodevices. *Nano Letters* 8, 3766-3770, https://doi.org/10.1021/nl802086x (2008).
- Zenhausern, F., O'Boyle, M. P. & Wickramasinghe, H. K. Apertureless near-field optical microscope. *Applied Physics Letters* 65, 1623-1625, https://doi.org/10.1063/1.112931 (1994).
- Zenhausern, F., Martin, Y. & Wickramasinghe, H. K. Scanning Interferometric Apertureless Microscopy: Optical Imaging at 10 Angstrom Resolution. *Science* 269, 1083-1085, https://doi. org/10.1126/science.269.5227.1083 (1995).
- Keilmann, F., Huber, A. J. & Hillenbrand, R. Nanoscale Conductivity Contrast by Scattering-Type Near-Field Optical Microscopy in the Visible, Infrared and THz Domains. *Journal of Infrared, Millimeter, and Terahertz Waves* 30, 1255-1268, https://doi.org/10.1007/s10762-009-9525-3 (2009).
- von Ribbeck, H. G. et al. Spectroscopic THz near-field microscope. Opt. Express 16, 3430-3438, https://doi.org/10.1364/OE.16.003430 (2008).
- Joyce, H. J. et al. Electronic properties of GaAs, InAs and InP nanowires studied by terahertz spectroscopy. Nanotechnology 24, 214006, https://doi.org/10.1088/0957-4484/24/21/214006 (2013).
- Brehm, M., Taubner, T., Hillenbrand, R. & Keilmann, F. Infrared spectroscopic mapping of single nanoparticles and viruses at nanoscale resolution. *Nano Lett* 6, 1307-1310, https://doi.org/10.1021/nl0610836 (2006).
- Ritchie, E. T. et al. Mapping Free-Carriers in Multijunction Silicon Nanowires Using Infrared Near-Field Optical Microscopy. Nano Letters 17, 6591-6597, https://doi.org/10.1021/acs.nanolett.7b02340 (2017).
- Taubner, T., Hillenbrand, R. & Keilmann, F. Nanoscale polymer recognition by spectral signature in scattering infrared near-field microscopy. *Applied Physics Letters* 85, 5064-5066, https://doi.org/10.1063/1.1827334 (2004).
- 19. Chen, X. et al. THz Near-Field Imaging of Extreme Subwavelength Metal Structures. ACS Photonics 7, 687-694, https://doi.org/10.1021/acsphotonics.9b01534 (2020).



- Gao, Y. et al. Chiral terahertz wave emission from the Weyl semimetal TaAs. Nature Communications 11, 720, https://doi.org/10.1038/s41467-020-14463-1 (2020).
- Park, B. C. et al. Terahertz single conductance quantum and topological phase transitions in topological insulator Bi2Se3 ultrathin films. *Nature Communications* 6, 6552, https://doi.org/10. 1038/ncomms7552 (2015).
- 22. Wagner, M. *et al.* Ultrafast and Nanoscale Plasmonic Phenomena in Exfoliated Graphene Revealed by Infrared Pump–Probe Nanoscopy. *Nano Letters* **14**, 894-900, https://doi.org/10.1021/nl4042577 (2014).
- Jiang, T., Kravtsov, V., Tokman, M., Belyanin, A. & Raschke, M. B. Ultrafast coherent nonlinear nanooptics and nanoimaging of graphene. *Nature Nanotechnology* 14, 838-843, https://doi.org/ 10.1038/s41565-019-0515-x (2019).
- Kiwa, T., Tonouchi, M., Yamashita, M. & Kawase, K. Laser terahertz-emission microscope for inspecting electrical faults in integrated circuits. Opt. Lett. 28, 2058-2060, https://doi.org/10.1364/OL.28.002058 (2003).
- 25 Nakanishi, H. *et al.* Imaging of a Polycrystalline Silicon Solar Cell Using a Laser Terahertz Emission Microscope. *Applied Physics Express* **5**, 112301, https://doi.org/10.1143/apex.5.112301 (2012).
- 26 Tonouchi, M., Yamashita, M. & Hangyo, M. Terahertz radiation imaging of supercurrent distribution in vortex-penetrated YBa2Cu3O7-δ thin film strips. *Journal of Applied Physics* 87, 7366-7375, https://doi.org/10.1063/1.372995 (2000).
- 27. Pizzuto, A., Mittleman, D. M. & Klarskov, P. Laser THz emission nanoscopy and THz nanoscopy. *Opt Express* 28, 18778-18789, https://doi.org/10.1364/oe.382130 (2020).
- Klarskov, P., Kim, H., Colvin, V. L. & Mittleman, D. M. Nanoscale Laser Terahertz Emission Microscopy. ACS Photonics 4, 2676-2680, https://doi.org/10.1021/acsphotonics.7b00870 (2017).
- 29. Mooshammer, F. *et al.* Quantitative terahertz emission nanoscopy with multiresonant near-field probes. *Opt. Lett.* **46.** 3572-3575, https://doi.org/10.1364/OL.430400 (2021).
- Pizzuto, A. et al. Nonlocal Time-Resolved Terahertz Spectroscopy in the Near Field. ACS Photonics 8, 2904-2911, https://doi.org/10.1021/acsphotonics.1c01367 (2021).
- Li, P. et al. Collective near-field coupling and nonlocal phenomena in infrared-phononic metasurfaces for nano-light canalization. Nat Commun 11, 3663, https://doi.org/10.1038/s41467-020-17425-9 (2020).
- Chen, X. et al. Modern Scattering-Type Scanning Near-Field Optical Microscopy for Advanced Material Research. Advanced Materials 31, 1804774, https://doi.org/10.1002/adma.201804774 (2019).
- Mooshammer, F. et al. Quantifying Nanoscale Electromagnetic Fields in Near-Field Microscopy by Fourier Demodulation Analysis. ACS Photonics 7, 344-351, https://doi.org/10.1021/acsphotonics.9b01533 (2020).
- Beard, M. C., Turner, G. M. & Schmuttenmaer, C. A. Transient photoconductivity in GaAs as measured by time-resolved terahertz spectroscopy. *Physical Review B* 62, 15764-15777, https://doi.org/10.1103/PhysRevB.62.15764 (2000).
- 35. Hillenbrand, R. & Keilmann, F. Complex Optical Constants on a Subwavelength Scale. *Physical Review Letters* **85**, 3029-3032, https://doi.org/10.1103/PhysRevLett.85.3029 (2000).
- 36 Richards, D., Zayats, A., Keilmann, F. & Hillenbrand, R. Near-field microscopy by elastic light scattering from a tip. *Philosophical Transactions of the Royal Society of London. Series A: Mathematical, Physical and Engineering Sciences* 362, 787-805, https://doi.org/10.1098/rsta.2003.1347 (2004).
- HillenbRand, R., Knoll, B. & Keilmann, F. Pure optical contrast in scattering-type scanning near-field microscopy. *Journal of Microscopy* 202, 77-83, https://doi.org/10.1046/j.1365-2818.2001.00794.x (2001).
- Johnston, M. B., Whittaker, D. M., Corchia, A., Davies, A. G. & Linfield, E. H. Simulation of terahertz generation at semiconductor surfaces. *Physical Review B* 65, 165301, https://doi.org/ 10.1103/PhysRevB.65.165301 (2002).
- Castro-Camus, E., Lloyd-Hughes, J. & Johnston, M. B. Three-dimensional carrier-dynamics simulation of terahertz emission from photoconductive switches. *Physical Review B* 71, 195301, https://doi.org/10.1103/PhysRevB.71.195301 (2005).
- 40. Jackson JD. Classical electrodynamics. Third edition. Wiley (1999).

**Publisher's Note** Springer Nature remains neutral with regard to jurisdictional claims in published maps and institutional affiliations.

Springer Nature or its licensor (e.g. a society or other partner) holds exclusive rights to this article under a publishing agreement with the author(s) or other rightsholder(s); author self-archiving of the accepted manuscript version of this article is solely governed by the terms of such publishing agreement and applicable law.

